

Detecting the Cosmic Dipole Anisotropy in Large-Scale Radio Surveys

Fronefield Crawford¹

ABSTRACT

The detection of a dipole anisotropy in the sky distribution of sources in large-scale radio surveys can be used to constrain the magnitude and direction of our local motion with respect to an isotropically distributed extragalactic radio source population. Such a population is predicted to be present at cosmological redshifts in an isotropically expanding universe. The extragalactic radio source population is observed to have a median redshift of $z \sim 1$, a much later epoch than the cosmic microwave background ($z \sim 1100$). I consider the detectability of a velocity dipole anisotropy in radio surveys having a finite number of source counts. The statistical significance of a velocity dipole detection from radio source counts is also discussed in detail. I find that existing large-scale radio survey catalogs do not have a sufficient number of sources to detect the expected velocity dipole with statistical significance, even if survey masking and flux calibration complications can be completely eliminated (i.e., if both the surveys and observing instruments are perfect). However, a dipole anisotropy should be easily detectable in future radio surveys planned with next-generation radio facilities, such as the Low Frequency Array and the Square Kilometer Array; tight constraints on the dipole magnitude and direction should be possible if flux calibration problems can be sufficiently minimized or corrected and contamination from local sources eliminated.

Subject headings: methods: analytical – catalogs – large-scale structure of universe

1. Introduction and Motivation

The measurement of a dipole anisotropy in large-scale surveys can be used to probe the distribution of matter at different distances and constrain our local motion with respect to large-scale mass distributions in the universe. There have been a number of attempts to measure the dipole anisotropy in different surveys. The dipole anisotropy in the cosmic microwave background at redshift $z \sim 1100$, probed by the *Cosmic Background Explorer* (Smoot et al. 1992), and more recently by the *Wilkinson Microwave Anisotropy Probe* (Bennett et al. 2003), was clearly detected, and tight

¹Department of Physics and Astronomy, Franklin & Marshall College, Lancaster, PA 17064; email: fcrawfor@fandm.edu

constraints on our local motion with respect to this background were made with these measurements. Analysis of the X-ray background at intermediate redshifts ($z \lesssim 4$) (Boughn et al. 2002) and the matter distribution at local distances (the Local Group), probed at infrared wavelengths using data from the *Infrared Astronomical Satellite* (IRAS) (Webster et al. 1997), have resulted in dipole detections as well. A marginal detection was also reported by Blake & Wall (2002) using radio data from the NRAO VLA Sky Survey (NVSS) (Condon et al. 1998). In Section 4.2, I discuss this radio survey specifically in the context of a dipole measurement. Baleisis et al. (1998) refer to a large number of previous dipole investigations using infrared galaxy catalogs (e.g., Meiksin & Davis 1986; Yahil et al. 1986; Villumsen & Strauss 1987; Harmon et al. 1987), optical catalogs (e.g., Lahav 1987; Lahav et al. 1988; Plionis 1988), IRAS redshift surveys (e.g., Rowan-Robinson et al. 1990; Strauss et al. 1992; Webster et al. 1997), and optical redshifts (Lynden-Bell et al. 1989; Hudson 1993). More details about inhomogeneities on large scales in different kinds of surveys can be found in Lahav (2000), where an extensive discussion is presented.

An isotropically distributed population of radio sources is predicted to exist at cosmological redshifts in an isotropically expanding universe. The extragalactic radio source population is observed to have a median redshift of $z \sim 1$ (e.g., Loan, Wall, & Lahav 1997), a much later epoch than the cosmic microwave background. Assuming the radio source distribution is intrinsically isotropic, our local motion with respect to the rest frame of this population would produce a dipole anisotropy in the sky distribution of radio sources. Large-scale radio survey catalogs covering a large fraction of the sky can in principle be used to detect this dipole anisotropy and subsequently constrain the magnitude and direction of our local motion with respect to this frame.

In this paper, I first describe the dipole anisotropy in the sky distribution of radio sources that would be introduced by our motion with respect to an isotropic radio source population. I then describe the corresponding dipole signal that would be seen in the distribution of discrete radio survey source counts. I describe a method to detect this signal in radio survey catalogs, with particular attention to the statistical significance of a possible detection. Finally, I consider both existing and proposed future radio surveys and whether a velocity dipole signal would be detectable with statistical confidence using this method given the number of discrete source counts present in these surveys. In this analysis, I consider only the most optimistic case in which there are no survey calibration problems, complications from the masking of certain survey regions, or uneven survey coverage.

2. The Effect of Motion on the Observed Radio Source Distribution

Motion with respect to the rest frame of an isotropic distribution of radio sources introduces two effects that change the observed source number density on the sky as a function of sky position (Ellis & Baldwin 1984; Condon 1988). The first effect is a boosting of the flux from sources located toward the direction of motion. This depends on the observer speed and the source spectral index. This Doppler effect changes the number of detectable sources above a given flux threshold in a radio

survey. The second effect, relativistic beaming, changes the apparent solid angle on the celestial sphere as seen by the moving observer. This in turn alters the observed source number density as a function of sky position. For N radio sources that are isotropically distributed across the full 4π sr of sky, the source number density is $\sigma_0 = N/4\pi$, a constant. The density variation from the observer’s motion will depend on the angle θ measured from the direction of motion (defined as $\theta = 0$) so that $\sigma(\theta) = dN/d\Omega$. Azimuthal symmetry in the situation removes any dependence on the second angle ϕ .

By combining the two effects described above, an expression for the source number density of radio sources seen by the moving observer has been presented by Ellis & Baldwin (1984). For small observer speeds ($\beta \equiv v/c \ll 1$) in which only first-order terms in β are retained, the source number density as a function of θ is shown to be:

$$\sigma(\theta) = \{1 + [2 + (\gamma - 1)(1 + \alpha)]\beta \cos \theta\}\sigma_0 \quad (1)$$

which is a dipole anisotropy. In this expression, γ is the power-law index for the number of extragalactic radio sources per flux interval ($dN/dS \sim S^{-\gamma}$), and α is the mean radio spectral index of the source population (defined here according to $S \sim \nu^{-\alpha}$). Following this, we can write:

$$\sigma(\theta) = (1 + A \cos \theta)\sigma_0, \quad (2)$$

where the amplitude $A = [2 + (\gamma - 1)(1 + \alpha)]\beta$. This expression (with some variation in nomenclature convention) has been used in the analysis of radio source counts by other authors (e.g. Condon 1988; Baleisis et al. 1998; Blake & Wall 2002). The mean values of the radio spectral index and power-law index for the extragalactic radio source population are estimated to be $\alpha \sim 0.75$, and $\gamma \sim 2$, respectively (e.g. Blake & Wall 2002), and I use these values in the analysis throughout the rest of the paper.

3. Detecting the Dipole Anisotropy in Radio Survey Catalogs

In this section, I describe a method for detecting the dipole anisotropy in radio survey catalogs, and I calculate the minimum number of discrete catalog sources required to detect the anisotropy with statistical significance. For the calculation, I assume complete sky coverage (4π sr) in which the survey has no masked, incomplete, or invalid regions. Perfect survey flux calibration is also assumed. These conditions, of course, do not apply in real surveys, and I briefly address (but do not solve) the complications posed by the presence of these effects, which can be quite significant. Since survey masking and flux thresholds will reduce the number of usable source counts in a survey, I do consider the effect that this reduction has on the dipole detectability in two of the surveys that I discuss.

3.1. A Method for Detecting the Dipole Anisotropy

A dipole vector \vec{D} can be measured for a distribution of discrete sources by computing an evenly weighted sum over all N source counts, where each source contributes a three-dimensional unit vector \hat{r} to the sum (e.g., Baleisis et al. 1998).² The direction of \hat{r} is determined by the position of the source on the sky as seen by the observer at the center of the celestial sphere. The sum is then:

$$\vec{D} = \sum_{i=1}^N \hat{r}_i \quad (3)$$

In the case of an ideal survey with perfect flux calibration, complete sky coverage, and in the limit of large N , all components of the vector sum would cancel except for a component along the direction of motion ($\theta = 0$), corresponding to the \hat{z} -axis.

In this case, the sum can be written as the integral of the number density over the celestial sphere:

$$\vec{D} = \hat{z} \int_{\phi=0}^{\phi=2\pi} \int_{\theta=0}^{\theta=\pi} \sigma(\theta) \cos \theta \sin \theta d\theta d\phi \quad (4)$$

The additional $\cos \theta$ term is present here since we are only concerned with the \hat{z} -component of the integral. Replacing $\sigma(\theta)$ in the expression with Equation 2 gives:

$$\vec{D} = \hat{z} \int_{\phi=0}^{\phi=2\pi} d\phi \int_{\theta=0}^{\theta=\pi} \sigma_0(1 + A \cos \theta) \cos \theta \sin \theta d\theta \quad (5)$$

which, when evaluated, gives:

$$\vec{D} = \frac{4\pi}{3} A \sigma_0 \hat{z} \quad (6)$$

Using $\sigma_0 = N/4\pi$ and $A = [2 + (\gamma - 1)(1 + \alpha)]\beta$, the magnitude of the measured dipole can be written as:

$$|\vec{D}| = D = \frac{1}{3} [2 + (\gamma - 1)(1 + \alpha)] \beta N \quad (7)$$

²There is abundant previous literature on the use of directional statistics and spherical data and coordinates (like those employed here) as applied across a number of scientific disciplines. Extensive discussions can be found in books by Batschelet (1981), Fisher et al. (1993), and Mardia & Jupp (1999) in which applications of directional statistics in a diverse range of subjects (e.g., biology, meteorology, psychology, earth sciences) are presented.

This is the dipole amplitude D one would measure for an ideal survey of N radio sources with complete sky coverage if the observer were moving with speed $v = \beta c$ (and $v \ll c$).

3.2. The Statistical Significance of a Dipole Detection

For a finite number of source counts N , there will be an uncertainty in the measured dipole \vec{D} arising from shot noise, and this uncertainty determines the significance with which \vec{D} can be measured. We can imagine the uncertainty as being represented by a three-dimensional spherical probability cloud in direction space which represents possible measured values of \vec{D} . This cloud will have some characteristic radial size, and it will be centered on the tip of the actual measured dipole \vec{D} . The cloud is spherical since there is an equal probability of the deviation occurring in any three-dimensional direction. This probability cloud can be used to estimate the uncertainty in the measured speed of the observer β , and exclude the zero-motion case ($\beta = 0$) at some confidence level (if an intrinsically isotropic distribution of radio sources is assumed). The direction of motion can also be determined, with statistical uncertainties, by considering the direction of \vec{D} and the angular size that the probability cloud subtends as seen from the origin (by the observer). For the test of whether the zero-motion case is excluded with statistical significance, it is functionally more useful to re-center the probability cloud at the origin instead of centering it at the tip of \vec{D} . This is done for the discussion below.

The characteristic size ρ of the probability cloud is determined by a random walk of N steps in three dimensions (corresponding to the N sources in the vector sum that produces \vec{D}). If the magnitude of each step is 1 unit (corresponding to the size of the unit vector), then we must consider the average magnitude of these steps as projected onto an axis. The actual step sizes along this axis will range from -1 to $+1$ with a probability weighting that is determined by the solid angle area from which the given projected value comes. The average projected step size s on the axis is computed from this to be $s = 1/\sqrt{3}$.

For large N , the probability distribution of the magnitude of the final radial displacement is determined by the three one-dimensional Gaussian distributions in Cartesian coordinates which represent the three directional degrees of freedom. The probability $p(r)$ that the displacement occurs at a radial distance r from the starting point (the origin) is:

$$p(r) = \frac{1}{\rho^3(2\pi)^{3/2}} 4\pi r^2 \exp(-r^2/2\rho^2) \quad (8)$$

This is obtained by multiplying the three one-dimensional Gaussian probability distributions and including an additional weighting factor $4\pi r^2$ to account for the increasing spherical volume element as r increases.

The characteristic size ρ is determined by the random walk according to:

$$\rho = s\sqrt{N} = \sqrt{\frac{N}{3}} \quad (9)$$

Using this, the probability $p(r)$ can be re-written in terms of N as:³

$$p(r) = \left(\frac{54}{\pi N^3}\right)^{1/2} r^2 \exp(-3r^2/2N) \quad (10)$$

Figure 1 shows the probability distribution $p(r)$ from Equation 10 plotted against a histogram of the magnitude of the displacement vectors D that were calculated from 10^5 simulated surveys. Each simulated survey had a random isotropic distribution of 2.7×10^4 sources (which is the number of sources selected for the analysis and discussion of the combined 87GB/PMN survey below; see also Table 1). One of the simulated surveys is shown in Figure 2 and is discussed in more detail below. The histogram in Figure 1 was produced from the set of displacement vectors shown in Figure 3 (this is discussed below), and it has been normalized in Figure 1 to have a total area equal to one for comparison with the probability curve. The match between the curve and the histogram supports the use of this probability distribution in the subsequent calculations and analysis.

We can use Equation 10 to estimate the likelihood of randomly measuring a dipole with a magnitude greater than or equal to D in the zero-motion, isotropic case. We integrate the probability function $p(r)$ from $r = D$ to an upper limit of $r = N$ (which is the maximum possible dipole value; in the limit of large N , the value of this upper limit approaches infinity). The integration is purely radial since the angular dependence drops out for the spherical cloud. The result of the integration, $p(r > D)$, which ranges between 0 and 1, is the probability-weighted volume outside of the radius D . This represents the likelihood of randomly measuring a dipole of magnitude D or greater from an isotropic source distribution. Conversely, we can use the measured dipole magnitude D to exclude the zero-motion case ($\beta = 0$) at a confidence level determined by $1 - p(r > D)$ (e.g., if $1 - p = 68\%$, then the zero-motion case would be excluded at the 1σ level).

We can also determine an uncertainty in the magnitude of the measured dipole D using similar reasoning. We surround the measured vector \vec{D} with the spherical probability cloud centered at its tip. We pick the confidence level of interest (1σ , 2σ , etc.; let us call it $n\sigma$) from the corresponding percentage level of exclusion. Using this, we solve for the corresponding radial distance r_n in the probability cloud for which the probability-weighted volume within r_n is the aforementioned percentage of the total probability-weighted volume. This is done by evaluating the integral for $p(r)$ using a lower limit (r_n) which will give the appropriate percentage level of exclusion. Once r_n has been determined in this way, this defines an $n\sigma$ error sphere centered on the tip of \vec{D} . Since

³This result is not new, and the same expression can be derived differently by computing the χ^2 probability distribution with three degrees of freedom, $\chi_3^2(3r^2/N)$. Introducing a change in variables with a Jacobian and employing a substitution eventually leads to a result that is identical to Equation 10.

the uncertainty cloud is spherical, the projection of the cloud onto the \hat{D} axis gives the magnitude r_n , which is the $n\sigma$ uncertainty in D . The measured dipole magnitude is then $D \pm r_n$ (at the $n\sigma$ confidence level). Figure 4 shows detection confidence levels of dipole detections for calculations of D and r_n from several idealized surveys with different numbers of source counts N and different assumed values for the dipole velocity β .

This error sphere can also be used to determine an uncertainty in the direction of \vec{D} . The projection of the error sphere onto the celestial sphere as seen by the observer at the center defines a circularly symmetric region on the sky centered on the dipole direction \hat{D} . Sky directions lying outside the circular region are statistically excluded at the $n\sigma$ level. Let the dipole direction \hat{D} correspond to $\theta = 0$ again, and let the $n\sigma$ angular uncertainty in the dipole direction be $\delta\theta_n$ (this is the angular radius of the projected circular region). $\delta\theta_n$ is determined by the angle between \hat{D} and a vector which starts at the origin and is tangent to the error sphere of radius r_n . This is calculated by:

$$\delta\theta_n = \arcsin(r_n/D) \quad (11)$$

for $r_n < D$. No statistically significant direction constraint can be made for the case $r_n \geq D$. This uncertainty angle $\delta\theta_n$ is determined by the number of sources N in the survey and the measured value of D (which in turn depends on N and the observer’s velocity β). Figure 5 shows calculations of $\delta\theta_n$ for an assumed dipole velocity of 370 km s^{-1} as a function of the number of survey source counts N .

3.3. Incomplete Survey Sky Coverage and Imperfect Flux Calibration

For real radio surveys which do not have complete sky coverage, an artificial dipole would be measured when the sum of the unit vectors \hat{r} is taken over the N observed sources. This dipole will be biased toward directions which have more complete survey coverage. To deal with this incompleteness when analyzing real radio survey data, one usually defines a mask of survey regions on the celestial sphere to exclude in the analysis. The vector sum is then taken over the distribution of sources in the unmasked, valid regions to obtain a measured dipole \vec{D} . The center of the uncertainty probability cloud (described above) will be offset from the origin (corresponding to a magnitude and direction) by an amount determined by the geometry of the unmasked region. In principle, one can simply subtract this offset vector from all other vectors in the analysis (such as the measured \vec{D}) so that everything (including the distribution of points in the probability cloud) is re-centered to the origin. One would then proceed with the analysis as described above.

However, even without any problems introduced by the flux calibration, the shapes of the regions to be masked in a real survey are generally complicated. For example, sources in the Galactic plane and in certain declination bands may not be appropriate to include in the analysis

(e.g., see the data masking used in the analysis of radio surveys by Loan, Wall, & Lahav (1997), Baleisis et al. (1998), and Blake & Wall (2002); see also Figure 2). Also, the finite number of sources introduces a shot noise uncertainty in the offset vector. In the absence of calibration issues, the most straightforward course of action would be to simulate the survey by randomly assigning positions to N sources drawn from an isotropic distribution within the unmasked region of the sky and compute the sum of source unit vectors for many of these simulations. Figure 2 shows an Aitoff projection in equatorial coordinates of a single simulated survey of 2.7×10^4 sources distributed isotropically over the unmasked regions of the sky (cf. Figure 1 of Baleisis et al. (1998) and their masked regions, which were used as a guide here). The set of resulting vector displacements from the survey simulations will produce a probability cloud in which the mean position defines the vector to be subtracted. Figure 3 shows the vector displacements produced from 10^5 simulated isotropic surveys like the one shown in Figure 2. In this plot, the mean vector has already been subtracted so that the cloud is centered at the origin, and the resulting displacements \vec{D} have been projected onto a two-dimensional plane. This distribution of displacements in Figure 3 is the probability cloud that was used to produce the histogram shown in Figure 1.

Source clustering at local distances can also affect the analysis of radio surveys (e.g., the NVSS Survey; see discussions by Boughn & Crittenden 2002, Blake and Wall 2002, and also below). In this paper I make the assumption that the intrinsic distribution of sources is homogeneous and that there is no significant clustering on large scales beyond the local mass distribution. I assume that local sources would be excised prior to analysis.

Also, real radio surveys do not have perfect flux calibration, and this can bias the source count distribution in certain sky regions, thereby producing an artificial dipole anisotropy. The effects of survey calibration errors in combination with the masking of survey regions can be quite severe, and dealing with these complex effects has been much discussed in the literature (e.g., Hivon et al. (2002) for the analysis of the cosmic microwave background, and Hamilton & Tegmark (2004) and Swanson et al. (2008) for large-scale galaxy catalogs, such as the Sloan Digital Sky Survey (York et al. 2000)). In the analysis presented here, I ignore all such calibration effects and consider only the raw source counts N and whether a dipole would be detectable in the idealized case where the surveys and instruments are perfect.

4. Prospects for a Dipole Detection in Existing and Proposed Future Radio Surveys

Large-scale radio surveys currently exist in which the method outlined here for detecting the velocity dipole can be applied. However, the statistical significance of such a detection depends on whether these surveys have a sufficient number of sources, even if the flux calibration were perfect. Next-generation radio instruments that are in various stages of planning and development will also be used to conduct large-scale radio surveys in the future. Below I consider existing and possible future radio surveys in the order of increasing number of source counts, and I discuss the possibility of detecting the dipole in each of the surveys in turn, assuming the most optimistic scenario (i.e.,

perfect flux calibration).

4.1. The 87 Green Bank and Parkes-MIT-NRAO Surveys

The 87 Green Bank (87GB) (Gregory & Condon 1991) and Parkes-MIT-NRAO (PMN) surveys (Griffith et al. 1994; Wright et al. 1994, 1996) were conducted at 4.85 GHz and covered the northern and southern celestial sky, respectively. Baleisis et al. (1998) and Loan, Wall, & Lahav (1997) give concise descriptions and summaries of these surveys in the context of large-scale structure and the velocity dipole effect, and they refer to a number of previous attempts to detect the velocity dipole (see also the references in Section 1). Baleisis et al. (1998) have conducted an analysis of whether the 87GB and PMN surveys could be used for detecting the dipole using a method similar to the one described here (in their case, they considered the measured dipole magnitude relative to the shot noise term but did not do a more extensive analysis of possible detection significance).

In their analysis, Baleisis et al. (1998) excised certain incomplete or unreliable survey regions identified by Loan, Wall, & Lahav (1997), including sky regions within 10° of the Galactic plane, to eliminate Galactic sources, and they imposed a minimum flux density cutoff of 50 mJy for sources to be considered. This latter selection reduced declination-dependent number density variations. After performing a similar excision (but retaining only sources between 50 and 100 mJy), I find that the selected sample consists of $\sim 2.7 \times 10^4$ sources covering $\sim 70\%$ of the celestial sphere (see Table 1). Figure 2 shows similar masking used in a simulated survey of 2.7×10^4 isotropically distributed sources. As was also found by Baleisis et al. (1998), I find that this is not an adequate number of source counts for a statistically significant dipole detection given the expected local velocity of $v \sim 370 \text{ km s}^{-1}$, even if these surveys had perfect flux calibration. As seen in Figure 4, an observer velocity that is an order of magnitude greater than this would be required for even a 3σ detection. Figure 5 shows that for the expected velocity, no direction constraint could be made with this sample at any significance level. The shot noise analysis conducted by Baleisis et al. (1998) showed that at least $\sim 4 \times 10^5$ galaxies over the sky would be needed to detect the velocity dipole at the same level as the shot noise (i.e., a 1σ detection). Our results are consistent with theirs and suggest a comparable number of sources would be needed for a 1σ detection (see Figure 4 and Table 1, particularly the NVSS select survey that has $\sim 3.1 \times 10^5$ sources). This result does not account for the dipole introduced from large-scale structure, which complicates the analysis further. Thus, the 87GB and PMN surveys are not adequate for detecting a velocity dipole anisotropy using this method, regardless of whether slightly different flux density selection criteria are used in the data selection.

4.2. The NRAO VLA Sky Survey

The NVSS is a large-scale radio survey that was conducted with the Very Large Array at 1.4 GHz (Condon et al. 1998). The total number of sources in the NVSS is $\sim 1.8 \times 10^6$, and the survey is estimated to be 99% complete down to an integrated flux density of 3.5 mJy. The survey covers 82% of the celestial sphere, corresponding to a declination range $\delta > -40^\circ$, and the majority of the sources in the survey are believed to be at cosmological distances.

Blake & Wall (2002) have searched the NVSS for a dipole anisotropy, and we follow their work to determine which survey regions and flux ranges could be considered reliable for the dipole search described here. Regions within 15° of the Galactic plane were masked by Blake & Wall (2002) to eliminate Galactic sources in their dipole analysis. They also eliminated the “clustering dipole” (from the Local Supercluster), which has its own dipole component, thereby ensuring that only cosmological sources were used in the analysis. This was done by eliminating radio sources within $30''$ of nearby galaxies known from several catalogs. Although the claimed 99% completeness level of the NVSS is 3.5 mJy (Condon et al. 1998), there are significant declination effects evident at this flux level in which the number density fluctuates by a few percent from the mean. Blake & Wall (2002) use a minimum flux cutoff of 15 mJy for their analysis (see their Table 1), which reduces the variations to less than 1%. However, as described above, these flux variations in combination with survey masking may still introduce complications which can significantly contaminate a dipole search.

After eliminating unreliable survey regions, Blake & Wall (2002) retained a selected sample of $\sim 3.1 \times 10^5$ sources above 15 mJy, representing $\sim 20\%$ of the initial sample (see Table 1). This is not adequate for a statistically significant dipole detection with the method presented here, even if flux calibration were perfect in the survey. For an expected dipole velocity of 370 km s^{-1} , the best possible dipole detection would be slightly less than 1σ (Figure 4). The dipole direction would also be unconstrained (Figure 5). Given these issues, I conclude that the NVSS cannot be used for detecting the velocity dipole using this method. Including all of the sources in the entire NVSS catalog ($N \sim 1.8 \times 10^6$) would yield a marginal detection and constraint at best ($\sim 3\sigma$), but flux calibration problems with the weakest sources in the survey prevent this from being feasible.

4.3. Next-generation Surveys with LOFAR and the SKA

Future large-scale radio surveys will be conducted with next-generation radio telescope facilities that are currently in various stages of planning and development. Among these new instruments are the Long Wavelength Array (LWA)⁴ (e.g., Taylor 2006), the Murchison Widefield Array (MWA)⁵

⁴<http://lwa.unm.edu>

⁵<http://www.haystack.mit.edu/mwa>

(e.g., Morales et al. 2006), and the Low Frequency Array (LOFAR)⁶, all of which will observe the sky at low radio frequencies (a few hundred MHz or less). Farther into the future, an even more advanced radio facility, the Square Kilometer Array (SKA)⁷, is being considered for development. Although the details of the surveys to be conducted with these instruments are not yet firmly established, I focus on two possible surveys that have been outlined for two of these instruments: LOFAR and the SKA.

LOFAR is an advanced radio telescope array that is expected to operate at low radio frequencies (30 to 240 MHz) and will have thousands of antenna elements distributed over hundreds of kilometers (e.g., Stappers et al. 2007; Falcke et al. 2007; Fender et al. 2008). A survey using LOFAR to search for gravitational lenses has been outlined by Jackson⁸. In a possible LOFAR survey, half of the celestial sky (2π sr) would be covered down to a limiting sensitivity of ~ 0.7 mJy at 151 MHz. The total number of sources expected to be detected in such a survey would be $\sim 3.5 \times 10^8$ (Table 1). Other recent estimates of source counts from proposed LOFAR surveys at a variety of wavelengths suggest a range of $\sim 10^7$ to $\sim 10^9$ detectable sources in 2π sr of sky (see, for example, the presentation by Rottgering 2007). For the sake of simplicity, we use the survey parameters outlined by Jackson for our analysis in which the expected number of source counts falls near the middle of this range.

The SKA is a planned next-generation radio telescope facility which will have vastly increased sensitivity for large-scale radio surveys. Simulations of a large-scale 1.4 GHz radio survey with the SKA suggest a limiting flux density of ~ 0.1 μ Jy and a yield of $\sim 10^9$ or more sources per sr (Hopkins et al. 1999, 2000). This corresponds to $\sim 10^{10}$ sources for the entire celestial sphere (Table 1).

Even with large gaps in sky coverage, the sheer number of sources in a survey conducted with either LOFAR or the SKA would far exceed the requirements for a statistically significant dipole detection with this method. If flux calibration problems can be sufficiently minimized or properly corrected, and if local source contamination can be removed, it should be easy to detect the dipole with large statistical significance if the dipole velocity is near the expected value of $v \sim 370$ km s⁻¹ (see Figure 4). The constraint on the dipole direction should also be very precise (Figure 5), easily constrained to within a few degrees or less in both cases.

⁶<http://www.lofar.org>

⁷<http://www.skatelescope.org>

⁸N. Jackson, LOFAR Memorandum Series #4

5. Conclusions

I have described a method for detecting a velocity dipole anisotropy in large-scale radio surveys and considered the feasibility of detecting this dipole with statistical significance in existing and proposed future large-scale surveys. This analysis does not account in any way for the severe complications that arise from imperfect flux calibration and masking effects in surveys, and therefore corresponds to the most optimistic detection case possible. Neither the combined 87GB/PMN survey nor the NVSS has a sufficient number of sources to detect the velocity dipole anisotropy with statistical significance using this method, even if no calibration or sample bias effects were present. However, proposed large-scale radio surveys using next-generation radio science instruments (e.g., LOFAR and the SKA) are more promising: surveys with these instruments should easily have enough source counts for a statistically significant dipole detection and direction constraint if flux calibration problems and contamination from local sources can be sufficiently reduced or eliminated.

I thank Elizabeth Praton for assistance with some of the derivations, Nathan Keim for contributions to the simulation work, and Steve Boughn and the referee John Ralston for helpful comments and insights which have improved this work.

REFERENCES

- Baleisis, A., Lahav, O., Loan, A. J., & Wall, J. V. 1998, *MNRAS*, 297, 545
- Batschelet, E. 1981, *Circular Statistics in Biology* (London: Academic Press)
- Bennett, C. L., et al. 2003, *ApJS*, 148, 1
- Blake, C. & Wall, J. 2002, *Nature*, 416, 150
- Boughn, S. P., & Crittenden, R. G. 2002, *Physical Review Letters*, 88, 021302
- Boughn, S. P., Crittenden, R. G., & Koehrsen, G. P. 2002, *ApJ*, 580, 672
- Condon, J. J. 1988, *Galactic and Extragalactic Radio Astronomy*, 641
- Condon, J. J., Cotton, W. D., Greisen, E. W., Yin, Q. F., Perley, R. A., Taylor, G. B., & Broderick, J. J. 1998, *AJ*, 115, 1693
- Ellis, G. F. R. & Baldwin, J. E. 1984, *MNRAS*, 206, 377
- Falcke, H. D., et al. 2007, *Highlights of Astronomy*, 14, 386
- Fender, R. et al. 2008, in *Bursts, Pulses, and Flickering: Wide-field Monitoring of the Dynamic Radio Sky*, *Proceedings of Science* (arXiv:0805:4349)

- Fisher, N. I., Lewis, T., & Embleton, B. J. J. 1993, *Statistical Analysis of Spherical Data* (Cambridge: Cambridge Univ. Press)
- Gregory, P. C. & Condon, J. J. 1991, *ApJS*, 75, 1011
- Griffith, M. R., Wright, A. E., Burke, B. F., & Ekers, R. D. 1994, *ApJS*, 90, 179
- Hamilton, A. J. S., & Tegmark, M. 2004, *MNRAS*, 349, 115
- Harmon, R. T., Lahav, O., & Meurs, E. J. A. 1987, *MNRAS*, 228, 5P
- Hivon, E., Górski, K. M., Netterfield, C. B., Crill, B. P., Prunet, S., & Hansen, F. 2002, *ApJ*, 567, 2
- Hopkins, A., Ekers, R., Jackson, C., Cram, L., Green, A., Manchester, R., Staveley-Smith, L., & Norris, R. 1999, *Publications of the Astronomical Society of Australia*, 16, 152
- Hopkins, A., Windhorst, R., Cram, L., & Ekers, R. 2000, *Experimental Astronomy*, 10, 419
- Hudson, M. J. 1993, *MNRAS*, 265, 72
- Lahav, O. 1987, *MNRAS*, 225, 213
- Lahav, O. 2000, *Cosmic Flows Workshop*, 201, 377
- Lahav, O., Rowan-Robinson, M., & Lynden-Bell, D. 1988, *MNRAS*, 234, 677
- Lineweaver, C. H., Tenorio, L., Smoot, G. F., Keegstra, P., Banday, A. J., & Lubin, P. 1996, *ApJ*, 470, 38
- Loan, A. J., Wall, J. V., & Lahav, O. 1997, *MNRAS*, 286, 994
- Lynden-Bell, D., Lahav, O., & Burstein, D. 1989, *MNRAS*, 241, 325
- Mardia, K. V. & Jupp, P. E. 1999, *Directional Statistics* (Chichester: Wiley)
- Meiksin, A., & Davis, M. 1986, *AJ*, 91, 191
- Morales, M. F., Bowman, J. D., Cappallo, R., Hewitt, J. N., & Lonsdale, C. J. 2006, *New Astronomy Review*, 50, 173
- Plionis, M. 1988, *MNRAS*, 234, 401
- Rottgering, H. 2007, in *Astrophysics in the LOFAR Era*, Emmen, Netherlands
- Rowan-Robinson, M., et al. 1990, *MNRAS*, 247, 1
- Smoot, G. F., et al. 1992, *ApJ*, 396, L1

- Stappers, B. W., van Leeuwen, A. G. J., Kramer, M., Stinebring, D., Hessels, J. 2007, in Proceedings of the 363. WE-Heraeus Seminar on Neutron Stars and Pulsars, 100
- Strauss, M. A., Yahil, A., Davis, M., Huchra, J. P., & Fisher, K. 1992, ApJ, 397, 395
- Swanson, M. E. C., Tegmark, M., Hamilton, A. J. S., & Hill, J. C. 2008, MNRAS, 387, 1391
- Taylor, G.B. 2006, in Long Wavelength Astrophysics, 26th Meeting of the IAU, Prague, Czech Republic, 12, 17
- Villumsen, J. V., & Strauss, M. A. 1987, ApJ, 322, 37
- Webster, M., Lahav, O., & Fisher, K. 1997, MNRAS, 287, 425
- Wright, A. E., Griffith, M. R., Burke, B. F., & Ekers, R. D. 1994, ApJS, 91, 111
- Wright, A. E., Griffith, M. R., Hunt, A. J., Troup, E., Burke, B. F., & Ekers, R. D. 1996, ApJS, 103, 145
- Yahil, A., Walker, D., & Rowan-Robinson, M. 1986, ApJ, 301, L1
- York, D. G., et al. 2000, AJ, 120, 1579

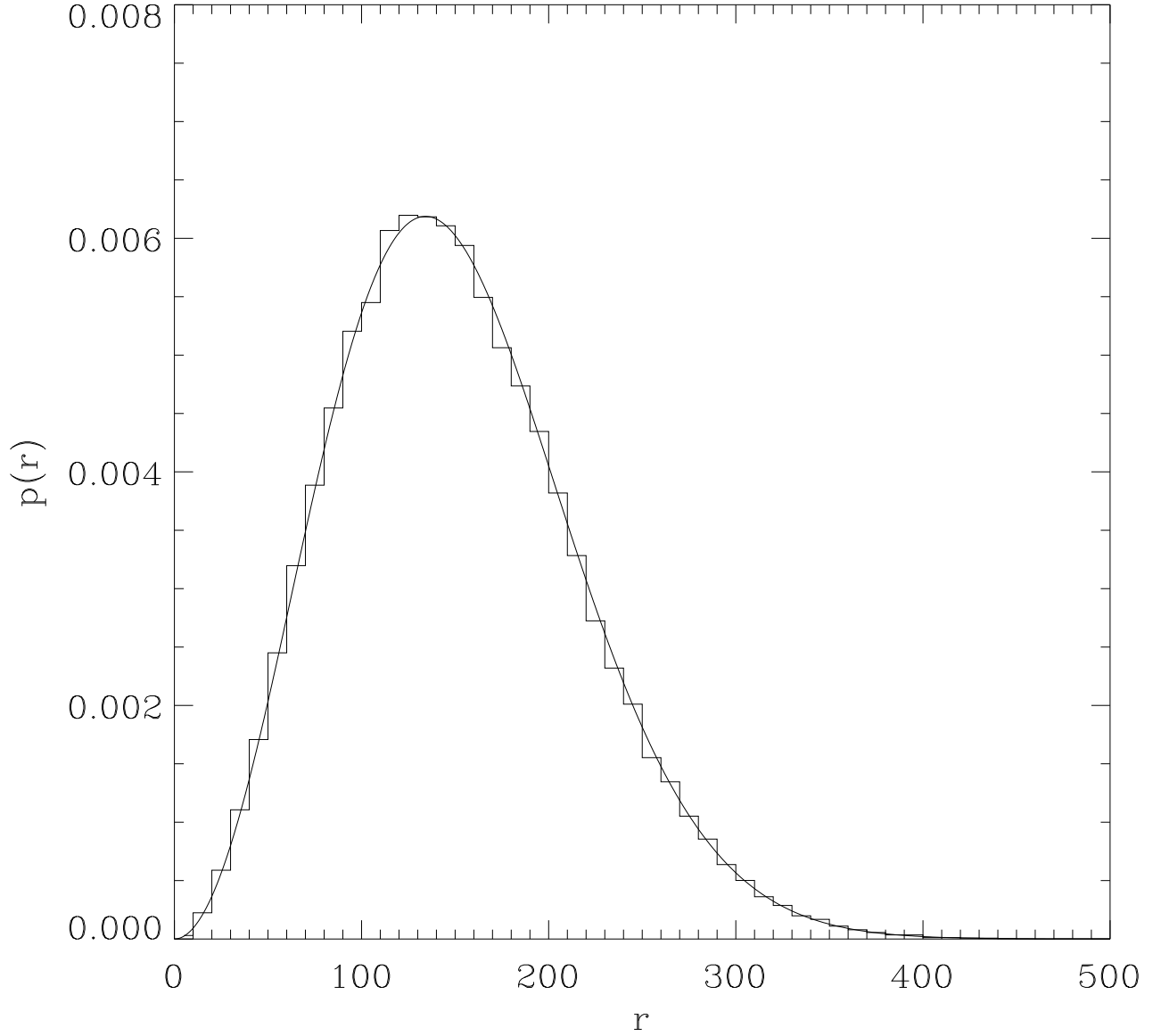


Fig. 1.— Histogram of the magnitude of the displacement vectors D calculated from 10^5 survey simulations, each of which had 2.7×10^4 sources isotropically distributed across the sky (see also Figure 3, from which this histogram was produced). Also plotted is the probability distribution $p(r)$ from Equation 10 as a function of radial displacement r , with $N = 2.7 \times 10^4$ used in the probability expression. The histogram has been normalized in the plot to have a total area equal to one for comparison with $p(r)$. The match between the curve and the histogram supports the use of this probability distribution in our analysis.

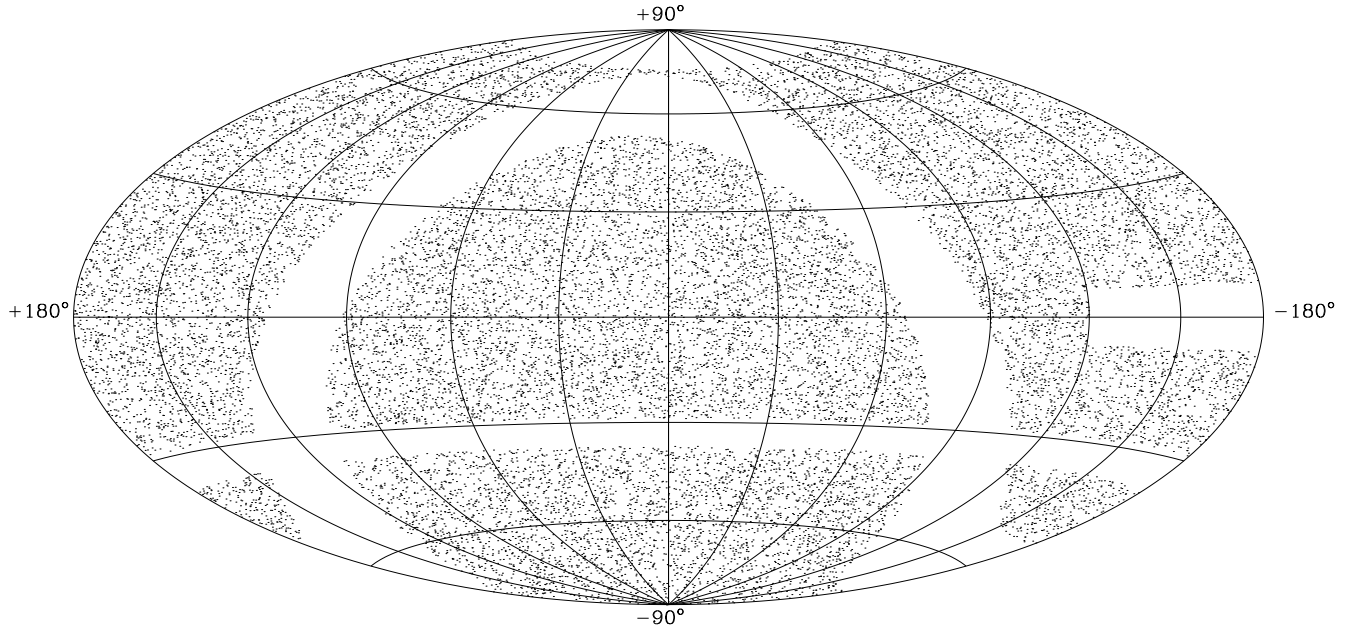


Fig. 2.— Aitoff projection plot in equatorial coordinates of 2.7×10^4 simulated radio sources distributed isotropically across the unmasked regions of the sky. The masked regions shown here are very close to the ones used by Loan, Wall, & Lahav (1997) and Baleisis et al. (1998) in their analysis of the combined 87GB/PMN survey (see also the discussion of these surveys in the text and Table 1). The 2.7×10^4 sources in this simulated survey correspond to the number of sources in the 87GB/PMN survey in the unmasked regions which have flux densities between 50 and 100 mJy. See Figure 1 of Baleisis et al. (1998) for a qualitative comparison of this simulated source distribution with the actual source distribution.

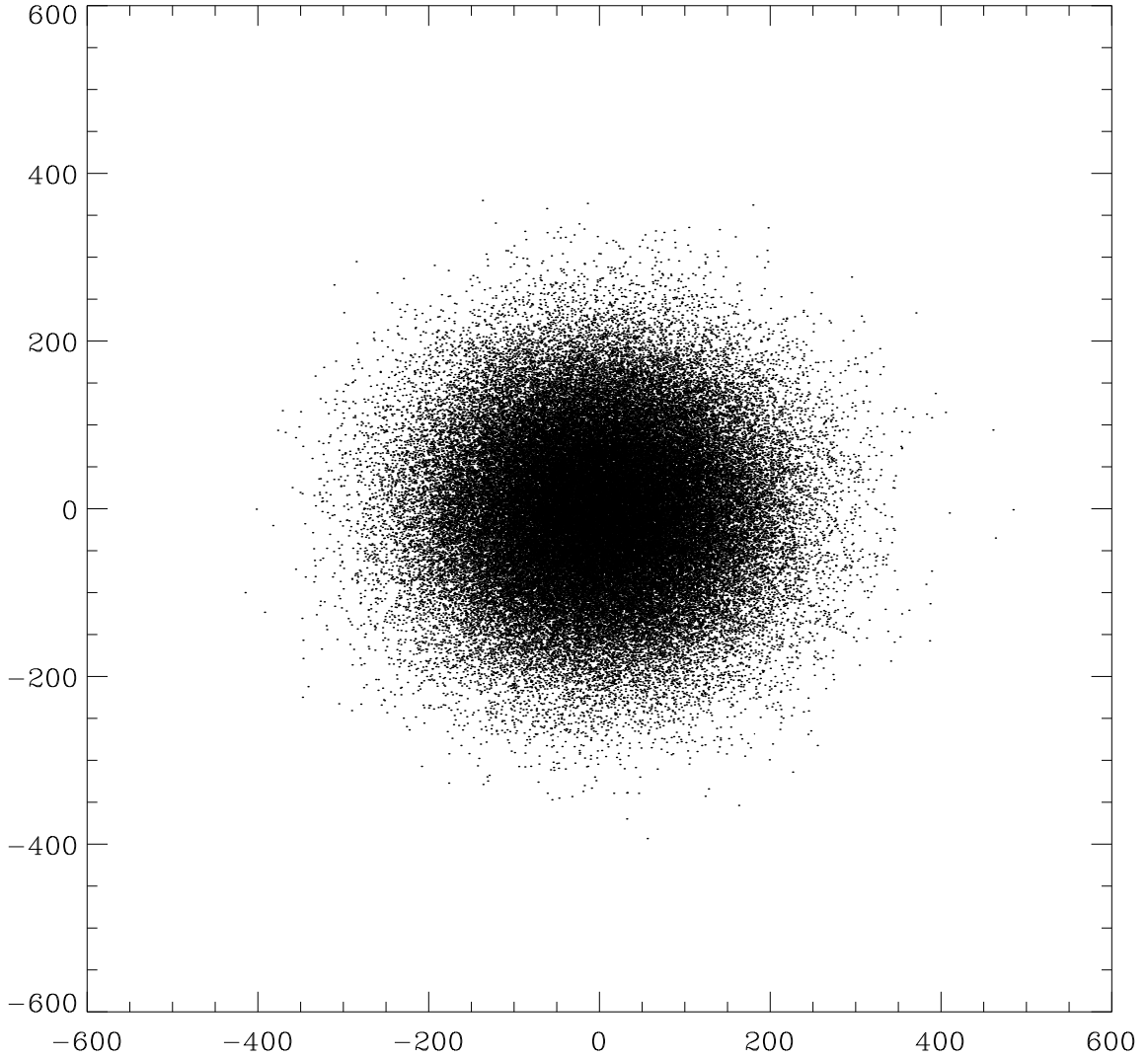


Fig. 3.— Two dimensional projection plot of the set of displacement vectors \vec{D} in three dimensions that were produced from 10^5 simulations of isotropic surveys, each of which had 2.7×10^4 sources. One of these simulated surveys is shown in Figure 2. The distribution shown here was produced after the mean of the distribution was subtracted from each displacement vector to correct for the vector offset introduced from survey masking effects. This three-dimensional distribution was used to produce the histogram of radial displacements shown in Figure 1.

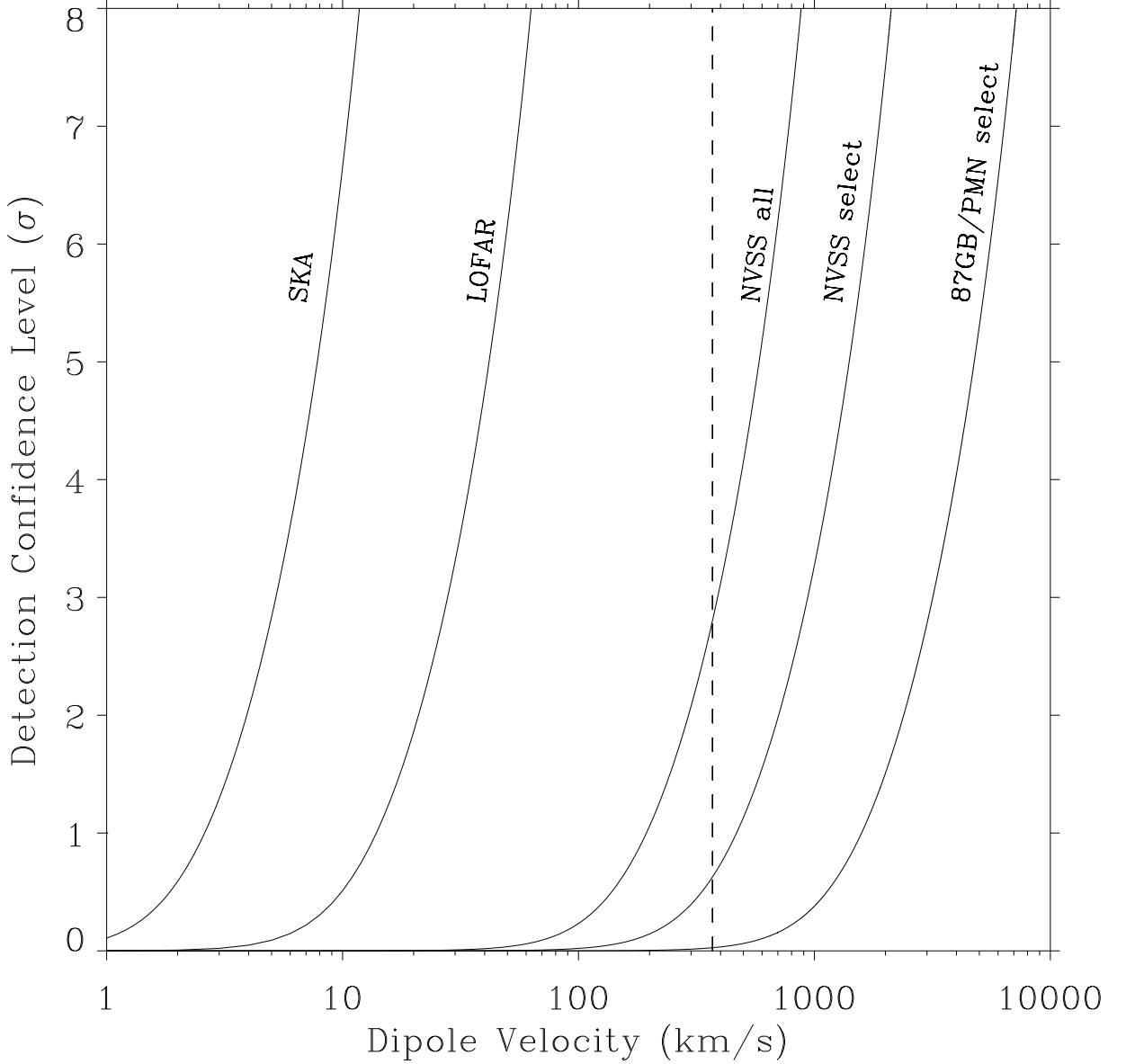


Fig. 4.— Dipole detection confidence level vs. dipole velocity for several existing and proposed future large-scale radio surveys. The solid curves represent the various surveys with different numbers of sources and are labeled (see the text and Table 1 for survey descriptions). In this plot, each survey is assumed to have perfect flux calibration and no contamination from local sources, corresponding to the most optimistic detection case possible. The expected dipole velocity of 370 km s^{-1} is indicated by the dashed vertical line. For this velocity, a minimum of 2.0×10^6 , 3.1×10^6 , and 4.5×10^6 survey sources would be required for 3σ , 4σ , and 5σ dipole detections, respectively.

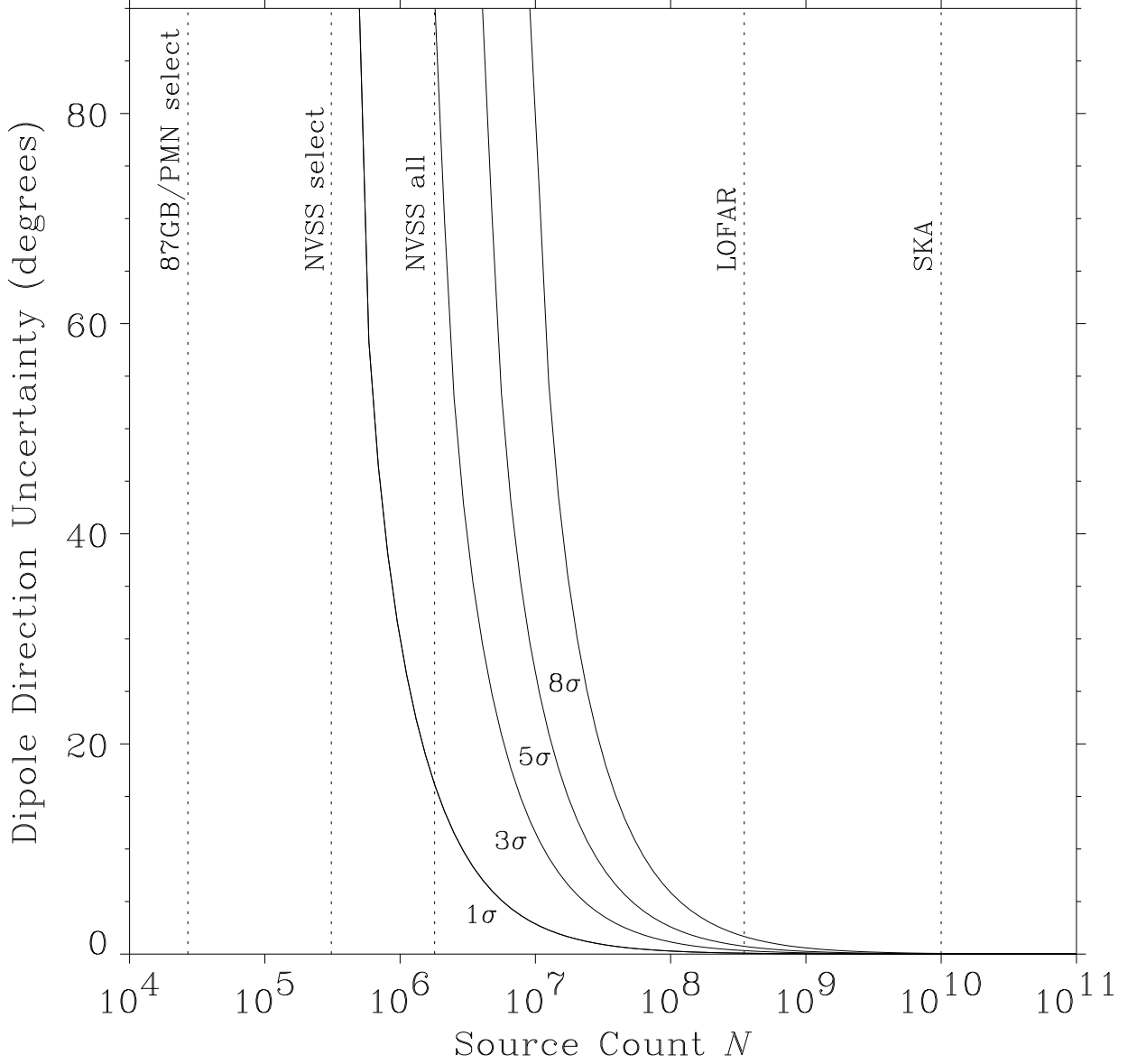


Fig. 5.— Uncertainty in the measured dipole direction ($\delta\theta$) vs. number of survey source counts (N) for several existing and proposed future large-scale radio surveys (see the text and Table 1). In this plot, a dipole velocity of 370 km s^{-1} is assumed as is perfect flux calibration and no contamination from local sources (corresponding to the most optimistic detection case possible). The dotted vertical lines represent the various surveys with different numbers of sources and are labeled. From left to right, the solid curves represent 1σ , 3σ , 5σ , and 8σ constraints on the dipole direction uncertainty that are possible with this detection method.

Table 1. Existing and Proposed Future Large-Scale Radio Surveys.

Radio Survey	Observing Frequency (GHz)	Flux Density Limit (mJy)	N
87GB/PMN select ^a	4.85	50	2.7×10^4
NVSS select ^b	1.4	15	3.1×10^5
NVSS all ^c	1.4	3.5	1.8×10^6
LOFAR ^d	0.15 ^f	0.7	3.5×10^8
SKA ^e	1.4 ^f	10^{-4}	$\sim 10^{10}$

Note. — “Select” refers to a selected sample of sources from the survey deemed appropriate for the analysis.

^aIncludes only sources with a flux density between 50 and 100 mJy from the combined 87GB and PMN surveys. Several regions, including regions within 10 degrees of the Galactic plane, were also excluded (Loan, Wall, & Lahav 1997; Baleisis et al. 1998).

^bIncludes only sources with a flux density above 15 mJy from the NVSS. Several regions, including regions within 15 degrees of the Galactic plane, were also excluded (Blake & Wall 2002).

^cIncludes all sources in the NVSS with a flux density above 3.5 mJy.

^dIncludes all sources in a possible LOFAR survey outlined by Jackson.

^eIncludes all sources in a possible SKA survey.

^fPossible observing frequency.